Geol. Mag. **140** (*4*), *2003, pp. 469–478. © 2003 Cambridge University Press*
DOI: 10.1017/S0016756803008094 *Printed in the United Kingdom*

New methods applied to the microstructure analysis of Messel oil shale: confocal laser scanning microscopy (CLSM) and environmental scanning electron microscopy (ESEM)

THOMAS NIX* & SUSANNE FEIST-BURKHARDT†

*Engineering Geology Division, Institute for Applied Geosciences, Darmstadt University of Technology, Schnittspahnstrasse 9, D-64287 Darmstadt, Germany
†Palaeontology Department, The Natural History Museum, Cromwell Road, London SW7 5BD, UK

(*Received* 6 January 2003; *accepted* 15 May 2003)

Abstract – Investigations of mass movements of the Messel oil shale in Germany presumed that swell- and especially shrink-deformations of the organic-rich clay were among the factors triggering initial displacements. Within the scope of the present studies, delicate clay/organic microstructures had to be deciphered. Reactions of clay minerals and microstructures upon dehydration were observed by environmental scanning electron microscopy (ESEM) and the distribution of organic matter was studied by confocal laser scanning microscopy (CLSM) in fluorescence mode. ESEM and CLSM have been demonstrated to be valuable tools for the microstructural characterization of laminated organic-rich sediments. The application of these analytical and imaging techniques will be of great interest to a wide range of geological disciplines such as palaeontology, organic petrology, engineering geology and global change studies.

Keywords: microstructure, black shale, laser methods, scanning electron microscopy, dehydration.

1. Introduction

The oil shale deposits of the Messel pit have become famous through the discovery of superbly preserved vertebrate fossils of Eocene age, and the controversial proposal to use the open mine pit as a waste disposal site after its closure for commercial use in the early 1970s (Schaal & Ziegler, 1992). Since 1995, when the Messel pit was placed on the UNESCO list of World Heritage sites, the government has taken over the responsibility for the site, including possible health and safety issues. These risks include mass movements of the artificial slopes of the former opencast mine, which may endanger surrounding buildings. In 1993 a geotechnical survey was initiated, with the aim to establish and settle the causes of the movements and to draw up a long-term stability forecast (Nix & Felder, 2002). Among other sources, swell- and especially shrink-deformations of the organic-rich clay were presumed to be one of the triggering factors for these mass movements. In order to test this hypothesis, a detailed microstructure analysis of the oil shale lithofacies-types involved has been carried out and the shrinking properties of the sediments have been identified. In addition to conventional transmitted light microscopy, fluorescence microscopy of thin sections and scanning electron microscopy, the sediment has been analysed using confocal laser scanning microscopy (CLSM) and environmental scanning electron microscopy (ESEM). The present contribution reports on the experience gained and results obtained by using these methods, which are new in the microstructure analysis of organic-rich sedimentary rocks.

* Author for correspondence: nix@geo.tu-darmstadt.de

2. Material

The Messel pit is situated about 20 km south of Frankfurt am Main, Hesse, Germany, near the cities of Darmstadt, Dieburg and Langen (Fig. 1). The sediments of the Eocene Messel Formation accumulated inside a volcanic crater lake, which was formed in Carboniferous igneous rocks and sediments from the Lower Permian (Harms *et al.* 1999; Nix & Felder, 2002). The Eocene Messel Formation (Franzen & Haubold, 1986) is subdivided lithostratigraphically from top to bottom into three units (Matthess, 1966; Weber & Hofmann, 1982): (1) Upper Messel Formation (dark clay at the base, grading upwards into light-coloured clays and sands); (2) Middle Messel Formation (Messel oil shale); (3) Lower Messel Formation (breccias, sandstones, siltstones, and clays with pyroclastic fragments).

The object of the present study is the oil shale of the Middle Messel Formation, which is a dark, organic-rich clay that bears the famous Messel fossils. Different lithotypes were distinguished by Franzen, Weber & Wuttke (1982) and Goth (1990) according to varying textures and sedimentary structures. For the purpose of

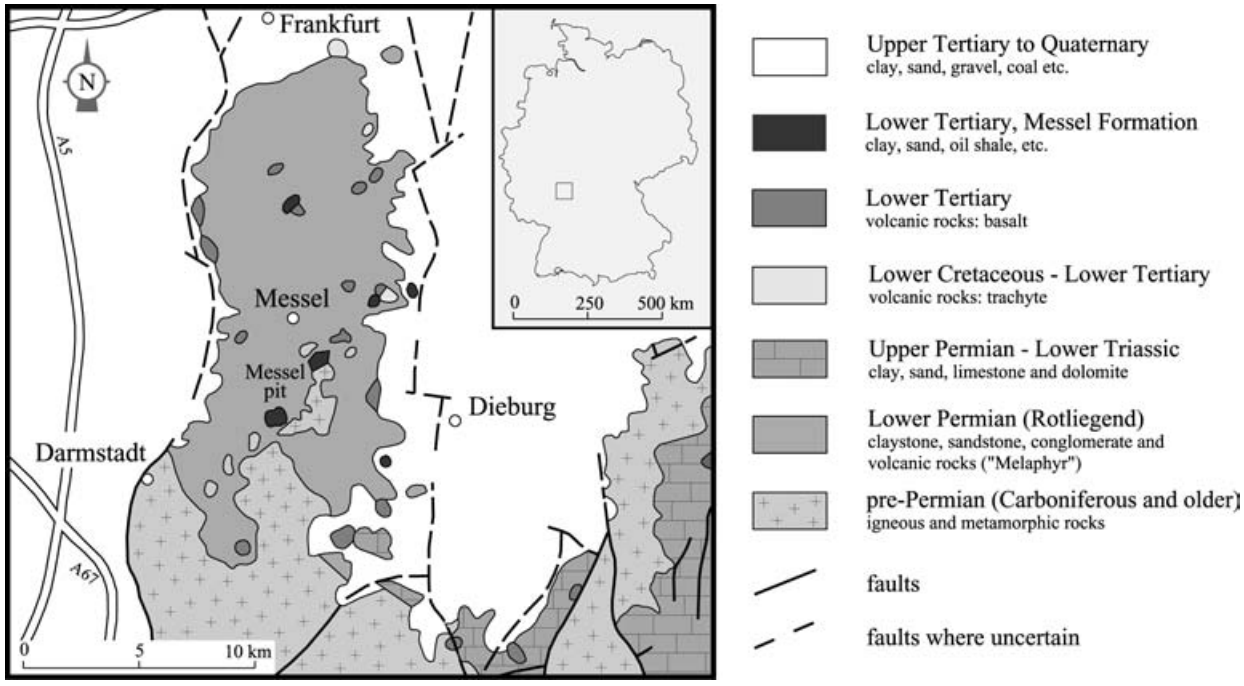

Figure 1. Geological and tectonic map of the Sprendlinger Horst in the South of Frankfurt (Hesse, Germany), and location of the Messel clay pit (adapted from Harms *et al*. 1999).

this study, two geotechnically significant lithofacies-types are differentiated: (1) lithofacies-type 1, a finely laminated, dark, organic-rich clay with occasional layers of siderite; and (2) lithofacies-type 2, a less well-bedded, dark, organic-rich clay.

The lamination in lithofacies-type 1 consists of alternations of clay mineral layers with variable amounts of organic components. The succession of organic-rich laminae and clay-rich interlaminae is formed by continuous sedimentation of the mineral phase and a rhythmic deposition of organic matter (Irion, 1977). Goth *et al*. (1988) showed that the main constituent of particulate organic matter and origin of the lamination are mass accumulations of cells of the green alga *Tetraedron minimum* (A. Braun) Hansgirg, 1888. Within the laminated parts of the Messel oil shale layers of siderite can often be found. Especially in areas at the margin of the former Messel lake, intercalations of sand and gravel occur. The massive and less well-bedded parts of the Messel oil shale (lithofacies-type 2) are interpreted as lake turbidites caused by tremors or sudden liquefaction of marginal deposits (Goth, 1990).

3. Methods

The microstructure of the Messel oil shale has been examined with conventional transmitted light microscopy (Figs 2a, 3a), scanning electron microscopy (SEM, Figs 2b–d, 3b–d) and fluorescence microscopy. The mineral composition has been analysed by X-ray powder diffraction. In addition to these conventional methods, confocal laser scanning microscopy (CLSM) was used to determine the distribution pattern and arrangement of organic matter, and dehydration experiments were carried out, using environmental scanning electron microscopy (ESEM). These two methods, CLSM and ESEM, are not novel in themselves, but they are applied here for the first time to the examination of organic components and dehydration studies of black shales.

3.a. Confocal laser scanning microscopy (CLSM)

The distribution of organic matter was very difficult to analyse in conventional fluorescence microscopy. For the purpose of this study, resolution in high magnification conventional fluorescence microscopy is not high enough (Jankowski & Littke, 1986) and images are blurred by the sediment's generally high content of fluorescing components. To decipher the delicate clay mineral to organic matter microstructures, ten samples of the Messel oil shale were examined using confocal laser scanning microscopy (CLSM) in fluorescence mode. CLSM has already been widely used in biological and medical applications (Sheppard & Shotton, 1997; Stevens, Mills & Trogadis, 1994; Pawley, 1995) as well as some biological oceanographic (Holloway & Cowan, 1997; Norton *et al*. 1998) and palaeontological studies (Feist-Burkhardt & Pross, 1999; Wilde & Schaarschmidt, 1993), but it has not previously been used in the field of microstructure analysis of organic-rich clay.

In CLSM a point light source is used to scan the object and excite fluorescence in the focal plane.

https://doi.org/10.1017/S0016756803008094 Published online by Cambridge University Press

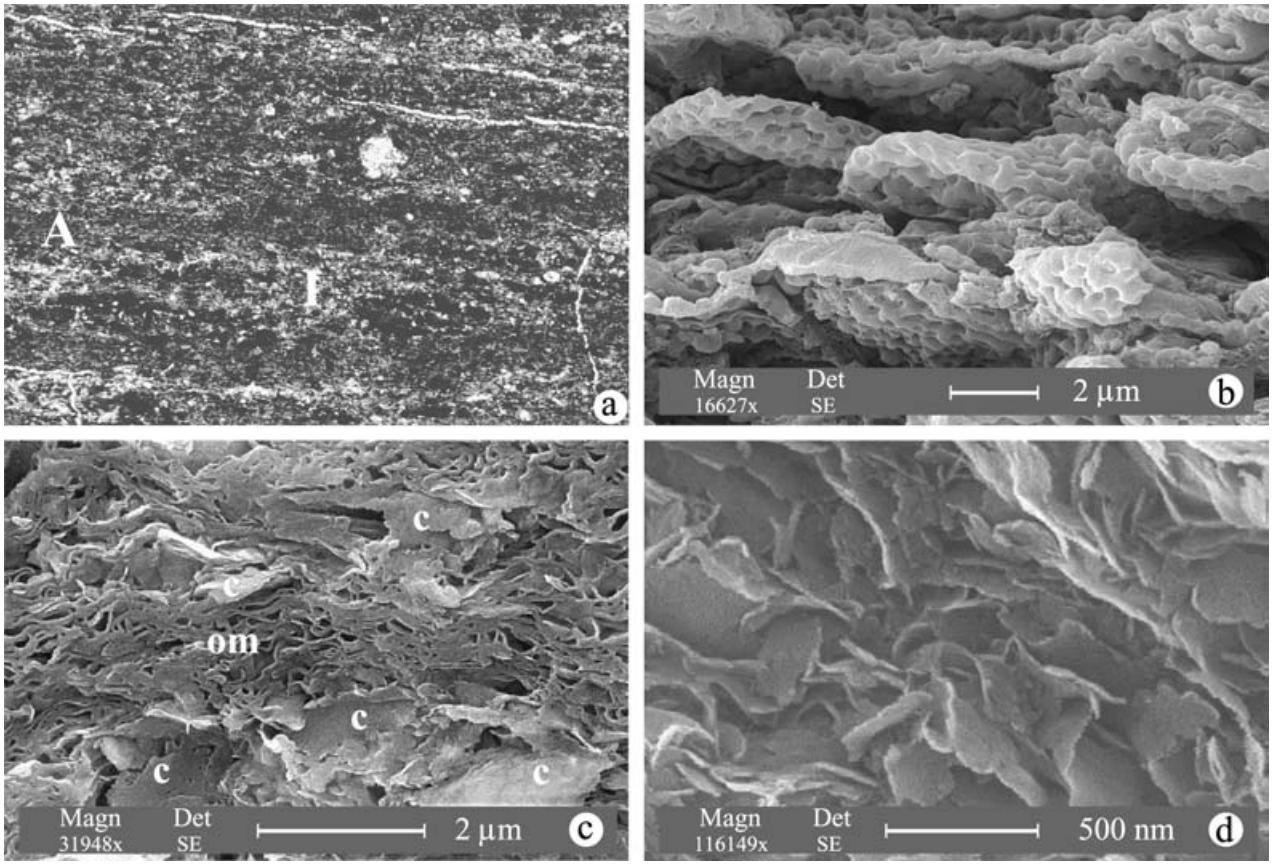

Figure 2. Laminated oil shale of the Middle Messel Formation, lithofacies-type 1. (a) Transmitted light micrograph of laminated oil shale with dark algal layers (A) and bright inorganic (mineral)-dominated layers (I). Thin section, image width 2.0 mm, height 1.3 mm. (b) HRSEM micrograph. Algal layer with horizontally arranged, slightly compressed algal cells of *Tetraedron minimum* (A. Braun) Hansgirg, 1888. *Tetraedron minimum* is characterized by a micropunctate to microreticulate surface ornament. Scale bar 2 μm. (c) HRSEM micrograph. Inorganic (mineral)-dominated layer with a mixture of (c) clay minerals (predominantly smectite) and deformed aggregates of clay minerals and (om) organic matter. Scale bar 2 μm. (d) HRSEM micrograph. Clay mineral layer with individual clay minerals associated by deformed edge to face contacts. Scale bar 500 nm.

The emitted fluorescence light is directed to a photomultiplier. The confocal arrangement with two fine pinhole apertures within the optical system ensures that only light from the selected focal plane reaches the detector. This accounts for the ability to take sharp, blur-free images of optical sections through a sample. The confocal arrangement is especially valuable in fluorescence microscopy, since stray light is almost completely eliminated and images with optimum resolution are produced. In subsequent steps of data processing, images of individual optical planes can be recombined to a single image showing a very high depth of focus, a so-called extended focus image. These datasets may be used to generate three-dimensional reconstructions and can be converted into stereoscopic images (Kehrel, 1999; Sheppard & Shotton, 1997).

All CLSM micrographs in this paper were taken with a Leica TCS NT confocal system on an inverted microscope, in fluorescence mode with a 63×1.32 n.A. water PL APO objective, an argon/krypton laser source and an image resolution of 512×512 pixels (Fig. 4b,c), and 1024×1024 pixels (Fig. 4a,d–f), respectively. Scanning methods and filter combinations used are the Leica software settings for FITC (fluorescein isothiocyanate), that is, an excitation wavelength of 488 nm and detection of an emission wavelength of 500 nm to 560 nm, and TRITC (tetramethyl rhodamine isothiocyanate), that is, an excitation wavelength of 568 nm and detection of an emission wavelength of 590 nm and longer. FITC (green) and TRITC (red) fluorescence has been detected simultaneously and is illustrated in overlay images (Fig. 4). No fluorescent dyes have been applied to the samples.

Conventional covered and uncovered thin-sections and knife-cut sediment blocks of about 1 cm edge-length were prepared for the analysis on the confocal microscope. The cube-shaped samples were analysed in specially prepared Petri dishes and were completely covered by water during the imaging sessions to prevent dehydration of the samples. The Petri dish was adapted by replacing the bottom of the dish with a standard thickness (17 μm) cover slip in order to allow high resolution imaging with the 63 $\times$ objective.

https://doi.org/10.1017/S0016756803008094 Published online by Cambridge University Press

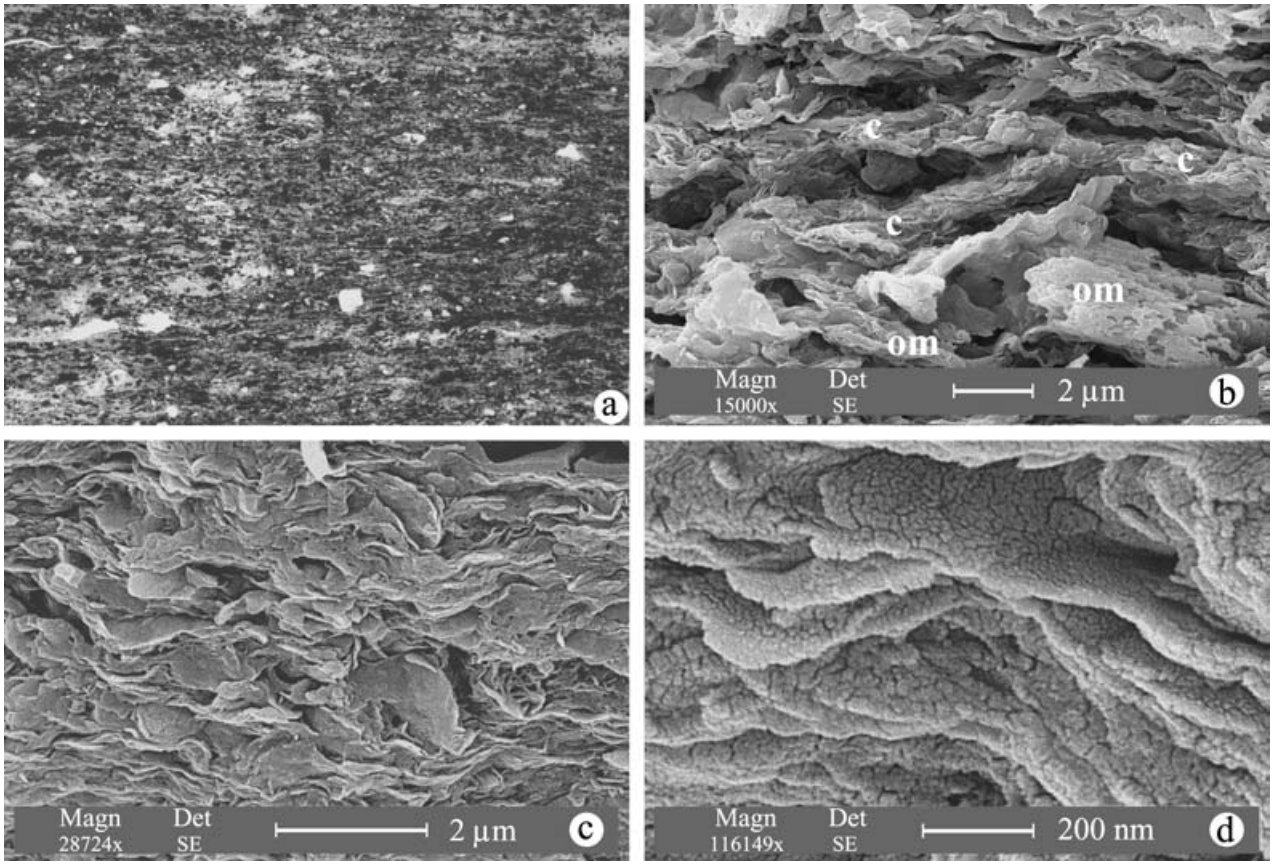

Figure 3. Massive, less well-bedded oil shale of the Middle Messel Formation, lithofacies-type 2. (a) Transmitted light micrograph of less well-bedded oil shale formed of a mixture of clay minerals and dispersed organic matter with some isolated quartz grains, lithoclasts and resedimented fragments of algal layers. Thin section, image width 4.9 mm, height 3.3 mm. (b) HRSEM micrograph. Sediment formed of a mixture of (c) clay minerals (predominantly smectite) and (om) organic matter (here fragments of single algal cells). Scale bar 2 μm. (c) HRSEM micrograph. Clay mineral crystals (predominantly smectite) associated by face to face contacts. Scale bar 2 μm. (d) HRSEM micrograph. Clay mineral crystals (smectite) associated by face to face contacts. At this very high magnification the gold coating on the surface of the clay minerals becomes visible as a granular cover. Scale bar 200 nm.

Use of an inverted microscope made it possible to analyse an almost undisturbed rock sample under water cover. This proved to be most important. The thin sections all showed artefacts of preparation, including: firstly, the rock sample had to be dried for placement onto the microscope slide, a process that produces alterations to the original undisturbed matrix and to the organic matter arrangement; secondly, the surface

Figure 4. Confocal laser scanning micrographs (CLSM) of the Middle Messel Formation oil shale. Double detection of green and red fluorescence illustrated in overlay images. (A) Algal layer, (I) inorganic-dominated layer, (T) *Tetraedron minimum* (A. Braun) Hansgirg 1888, (p) pollen grain, (fs) fluorescing sheath, (r) red, globular, fluorescing particle, (sfop) very small, fluorescing organic particles, (AOM) amorphous organic matter. (a) Lithofacies-type 1. Finely laminated oil shale with (A) green and yellow-orange algal layers at the lower and upper margin of the micrograph, and (I) an intercalated inorganic (mineral)-dominated layer. CLSM extended focus image, projection of 28 optical sections. Image size xy = 158 μm, z = 17.5 μm. (b) Lithofacies-type 1. (A) Algal layers with slightly compressed and horizontally arranged algal cells and (I) inorganic-dominated layer with dispersed organic matter. CLSM extended focus image, projection of 60 optical sections. Image size xy = 159 μm, z = 23.9 μm. (c) Lithofacies-type 1. Detail of (b). Thin algal layer (below) and layer rich in other organic detritus and AOM (above). Some algal cells (T) show the typical undulated surface arising from the micropunctate–microreticulate surface ornament. A single, thin and smooth-walled pollen grain, > 40 μm long, much larger than the algal cells of *Tetraedron*, is visible near the lower margin of the micrograph. CLSM extended focus image, projection of 54 optical sections. Image size xy = 79 μm, z = 19.3 μm. (d) Lithofacies-type 1. Detail of the transition zone from (A) an algal layer (below) to (I) an inorganic-dominated layer (above). Within the mineral matrix of the inorganic-dominated layer, figured organic particles (mainly *Tetraedron*), fluorescing fragments and amorphous organic matter are dispersed. CLSM extended focus image, projection of 45 optical sections. Image size xy = 44 μm, z = 16 μm. (e) Lithofacies-type 2. Large resedimented fragment of an algal layer with compressed algal cells and mineral enrichments (black) at the upper and lower margin of the micrograph. CLSM extended focus image, projection of 27 optical sections. Image size xy = 48 μm, z = 9.5 μm. (f) Lithofacies-type 2. Different fragments of figured organic particles and amorphous organic matter dispersed within the mineral matrix. CLSM extended focus image, projection of 45 optical sections. Image size xy = 43 μm, z = 16 μm.

https://doi.org/10.1017/S0016756803008094 Published online by Cambridge University Press

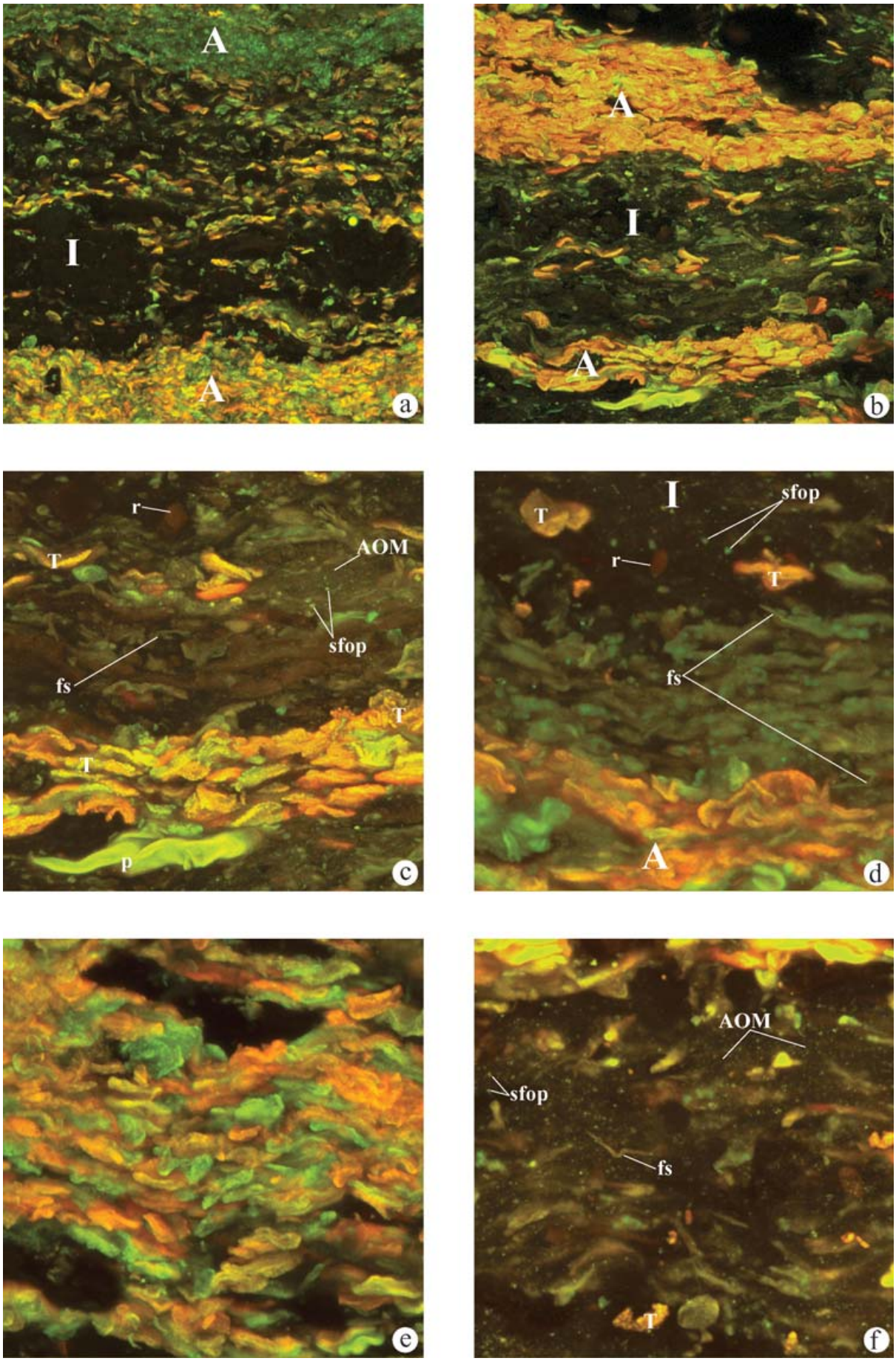

Figure 4. For legend see facing page.

https://doi.org/10.1017/S0016756803008094 Published online by Cambridge University Press

to analyse proved to be considerably disturbed, smeared or covered with tracks of grinding and polishing. By contrast, the cube-shaped sediment blocks were cut and broken with a knife to produce an almost undisturbed surface perpendicular to the bedding planes. During the time from collection of samples in the field to microscopical examination, the samples were continuously kept under water cover in order to keep possible alterations or microbial attack of the organic matter to a minimum. The naturally damp rock samples were covered with water from the mine immediately after collecting and stored in a watertight container. Microscopical examination was carried out within a day after collecting.

3.b. Scanning electron microscopy (HRSEM and ESEM)

The microstructure of the Messel oil shale was analysed using high-vacuum SEM, a well-known imaging technique, which has already been used in earlier investigations on the microfabric of shales (e.g. Macquaker & Gawthorpe, 1993; Kemp *et al*. 1998). The sample preparation for high-vacuum SEM requires elaborate and time-consuming preparation techniques. Ten samples were critical-point dried using ethanol as an intermediate fluid and CO_2 as transitional fluid. All samples were subsequently coated with gold.

To analyse the development of microstructural changes during dehydration, three samples of the Messel oil shale were examined using environmental scanning electron microscopy (ESEM). Environmental scanning electron microscopes are capable of secondary electron imaging of hydrated, wet samples and non-conducting, uncoated materials with a maximum resolution of 3.5 nm at 30 kV and a water vapour pressure of 10 mbar. No special sample preparation is needed. The presence of water vapour in the microscope chamber effects intrinsic induced signal amplification and charge neutralization. Secondary electrons, generated in the clay sample, collide with the water molecules, resulting in gaseous secondary electrons and positively charged ions. The gaseous secondary electrons further collide and significantly amplify the signal. The positive ions neutralize charge build-up on the clay sample surface, resulting in remarkable imaging capabilities. In low vacuum mode, secondary and backscattered electron images can be taken of uncoated and non-conductive materials (Danilatos, 1988; Reimer, 1998).

The high-vacuum SEM high-resolution micrographs in this paper (Figs 2b–d, 3b–d) were taken with a Philips XL30 HRSEM at the Department of Material Sciences, Darmstadt University of Technology, Germany. All ESEM micrographs (Figs 5a–d, 6a–d) were taken with a XL30 ESEM TMP, with tungsten filament, at Philips Electron Optics in Eindhoven, The Netherlands. The experiments were performed using a Peltier cooling stage to establish the right humidity and to prevent unintended dehydration of the samples. Variable information such as detector type, scale bar, mode and actual chamber pressure can all be found on the SEM-micrograph databar.

As explained in detail in Section 3.a, the samples were stored in water prior to examination. Microscopical analysis was carried out within a day of collecting.

4. Results

4.a. Microstructure of the Messel oil shale

In the oil shale of lithofacies-type 1, the fine lamination, caused by the rhythmic deposition of algal cells with a varying admixture of mineral matter, is clearly visible in transmitted light microscopy, scanning electron microscopy and confocal laser scanning microscopy (Figs 2–4). The darker, organic-dominated layers (A in Fig. 2a) are predominantly composed of individual cells of *Tetraedron minimum* (about 10 μm long and 2 μm thick, Figs 2b, 4a–c) almost without background sediment and reaching a thickness of up to 150–250 μm. Individual algal cells are horizontally arranged (Fig. 2b). The brighter layers (I in Fig. 2a) are mainly composed of clay minerals and organic matter. The clay minerals are predominantly small smectite crystals and grains (400–700 nm), with less frequent larger-sized illitic and kaolinitic material. Individual clay minerals are associated by edge to face contacts (Fig. 2d) and organic matter is embedded as deformed clay-organic aggregates (Fig. 2c). Occasionally, up to 50 μm thick pure clay mineral layers occur, which are composed almost exclusively of smectite. Siderite layers are intercalated occasionally and are made up of rod-shaped individual crystals, mixed with organic matter, opal-CT and pyrite. Other biogenic components reported to occur in the Messel oil shale are diatoms and sponge spicules (Heil, 1964), but these are relatively rare in the studied lithofacies-types.

Lithofacies-type 2 is a less well-bedded organic-rich clay (Fig. 3a). The sediment is formed of clay minerals and dispersed organic matter, mainly algal cells, with some isolated fine quartz grains, lithoclasts and resedimented fragments of algal layers. The clay mineral spectrum is dominated by smectite; illite and kaolinite occur infrequently. Individual clay minerals are associated frequently, in some cases exclusively, by face to face contacts (Figs 3c,d) and organic matter is embedded as clay-organic aggregates (Fig. 3b).

4.b. Distribution of organic matter

All samples of the Messel oil shale are characterized by a strong autofluorescence of the liptinite components (Fig. 4). Fluorescence excitation at two different wavelengths and double detection of emitted fluorescence has been used as a potential means to distinguish different liptinite components. The main fluorescing

https://doi.org/10.1017/S0016756803008094 Published online by Cambridge University Press

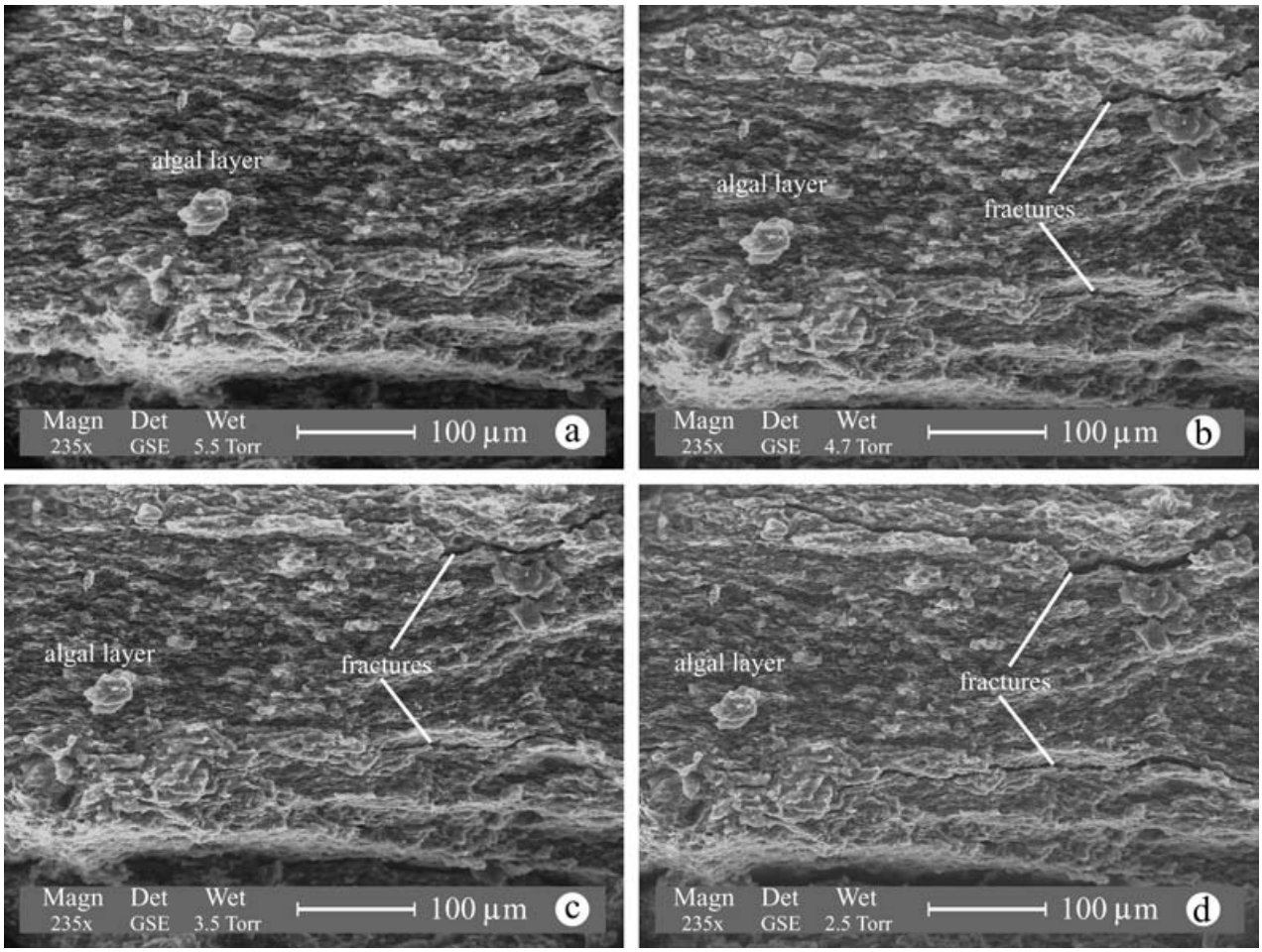

Figure 5. Dehydration series in ESEM micrographs, Middle Messel Formation, lithofacies-type 1. Algal layer (image centre) sandwiched by inorganic, mineral-dominated layers below and above. During dehydration, brittle fractures form within the transition zones. The fractures grow with increasing dehydration and increasing tensile stress. (a) to (d) Reduction of water vapour pressure from 5.5 to 2.5 torr. Scale bar 100 μm.

components in the samples are the algal cells of *Tetraedron minimum*. *Tetraedron* cells can be identified by a combination of features: their cushion-like morphology, homogeneous size and, at high magnifications, their typical micropunctate to microreticulate surface ornament giving a finely undulated aspect in the images perpendicular to the bedding plane (Figs 2b, 4c,e). The algal cells fluoresce at both excitation wavelengths over the entire spectrum detected and therefore show green and yellow-orange colours on the confocal images. Whether the cells appear green or orange depends on the thickness of algae present at the studied place and hence the total fluorescence intensity, but it is not necessarily an indicator for different organic composition. A few, much larger, thin-walled and smooth grains are present showing a green colour in the confocal images. These are interpreted as pollen grains (e.g. Fig. 4c).

Our results on the composition of the organic matter concur with the quantitative data of Jankowski & Littke (1986) and Rullkötter *et al*. (1988) who gave an average of 88 % liptinite, 10 % huminite and 2 % inertinite. Approximately 80–90 % of the liptinite in lithofacies-type 1 is deposited in these green and orange fluorescing dense organic algal layers (Fig. 4a–c). The remaining 10–20 % of liptinite is dispersed in the mineral matrix of inorganic-dominated layers, which are predominantly made up of non-fluorescing clay minerals (Fig. 4d). The dispersed organic matter within the inorganic-dominated layers, consists of mainly single *Tetraedron* cells, some few pollen grains or spores, other undetermined fluorescing figured organic particles or sheaths, and a few, very small, fluorescing organic particles (Figs 4b–d). Interstices between organic particles are filled with non-fluorescing clay minerals (mineral matrix; dark areas in Fig. 4d) and weakly fluorescing amorphous organic matter (unstructured organic matter derived from incomplete bacterial degradation of organic detritus).

Lithofacies-type 2 is predominantly made up of non-fluorescing mineral matter (clay minerals, fine quartz grains); organic matter is dispersed within the mineral matrix (Figs 4e,f). Main components of the organic matter are single *Tetraedron* cells, fragments of whole

https://doi.org/10.1017/S0016756803008094 Published online by Cambridge University Press

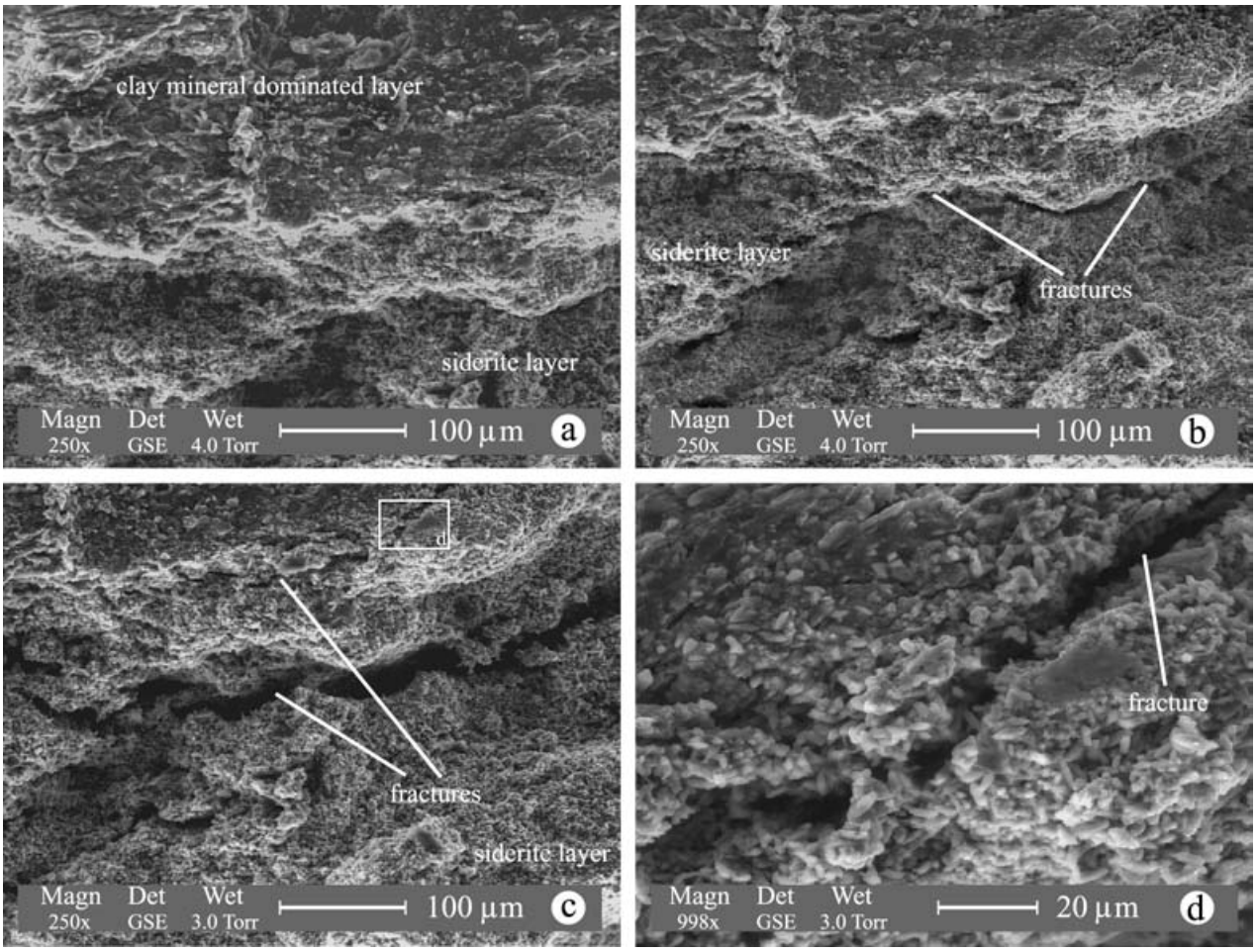

Figure 6. Dehydration series in ESEM micrographs, Middle Messel Formation, lithofacies-type 1. Transition zone of an inorganic, mineral-dominated layer (above) and a siderite layer (below). During dehydration, a brittle fracture forms within the transition zone. The fracture grows with increasing dehydration and increasing tensile stress. (a) to (c) Reduction of water vapour pressure from 4.0 to 3.0 torr. Scale bar 100 μm. (d) Detail of (c). Fracture within siderite layer, close to the transition from the clay mineral-dominated layer above. Scale bar 20 μm.

algal layers and very small fluorescing, organic fragments. Figure 4e shows a resedimented fragment of an algal layer. Additionally, pollen grains and spores, and other undetermined fluorescing figured organic particles may be present. Interstices between non-fluorescing clay minerals (mineral matrix, dark areas in Fig. 4f) are predominantly filled with weakly fluorescing amorphous organic matter.

4.c. Changes in microstructure by dehydration

The ESEM micrographs in Figures 5 and 6 show the dehydration series of a finely laminated lithofacies-type 1 sample. The horizontally deposited algal layer in the middle of Figure 5a–d is sandwiched by inorganic-dominated layers. Figure 6a–d documents the transition zone of an inorganic, clay mineral-dominated layer to a siderite layer.

By reducing the water vapour pressure from 5.5 to 2.5 torr (Fig. 5), and from 4.0 to 3.0 torr (Fig. 6), different humidity stages were established and deformation of the clay samples during one dehydration path has been observed (Figs 5a–d and 6a–d, respectively). During dehydration, fractures at the top and the bottom of the algal layer and at the transition zone of the siderite layer are formed. Stress maxima develop at inhomogeneities, between layers of different composition and different strength and deformation properties. With increasing tensile stress the materials tensile strength is exceeded and brittle fractures form at a right angle to the action line of stress, parallel to lamination.

5. Summary and conclusions

The microscopical examination of the oil shale of the Middle Messel Formation has shown that most of the constituent organic matter in lithofacies-type 1 is localized in discrete algal layers, which are, together with some thin siderite layers, responsible for the laminated aspect of the oil shale.

https://doi.org/10.1017/S0016756803008094 Published online by Cambridge University Press

Lithofacies-type 2 is dominated by clay minerals but also contains a significant proportion of organic matter. The organic matter and lumps of fragmented, resedimented algal layers are dispersed within the mineral matrix. Clay minerals are often covered by amorphous organic matter.

The ESEM analysis documented the formation of fractures during dehydration at the boundaries between adjacent layers of different composition: clay-dominated to algal layers, clay-dominated to siderite layers. With increasing tensile stress due to dehydration, brittle fractures develop at these inhomogeneities. These areas of distinct material change seem to be the places where the zones of weakness are created.

The study has further demonstrated that novel analytical and imaging techniques, ESEM and CLSM, can greatly contribute to the study of laminated organic-rich sediments, allowing identification of different organic and inorganic components and their spatial arrangement, and the characterization of microfacies. These techniques may be usefully employed in many different disciplines of Earth Sciences, from palaeontology to geotechnical studies, as demonstrated previously and herein, as well as in sedimentological applications, reaching from reservoir and source rock analysis to global change studies.

Acknowledgements. We would like to thank Philips Electron Optics in Eindhoven, The Netherlands, and Ellen Baken for enabling access to the ESEM and operating the instrument. The CLSM examinations were carried out at the facilities of the Biology Department, Institute of Zoology at Darmstadt University of Technology, Germany. The HRSEM examinations were carried out at the facilities of the Material Sciences Department at Darmstadt University of Technology, Germany. Thanks are also due to Dorothee Schroth (Leica Vertriebsgesellschaft, Bensheim, Germany) for her invaluable advice concerning operation of the Leica CLSM, image acquisition and further image processing and to Dr. A. Balogh (Darmstadt) for his training on the HRSEM. This study has been carried out while one of the authors (T.N.) held a research grant funded by the Hessian Geological Survey, Wiesbaden, Germany.

References

DANILATOS, G. D. 1988. Foundations of environmental scanning electron microscopy. *Advances in Electronics and Electron Physics* **71**, 109–250.

FEIST-BURKHARDT, S. & PROSS, J. 1999. Morphological analysis and description of Middle Jurassic dinoflagellate cyst marker species using confocal laser scanning microscopy, digital optical microscopy and conventional light microscopy. *Bulletin du Centre de Recherche Elf Exploration Production, 1998* **22**(1), 103–45.

FRANZEN, J. L., WEBER, J. & WUTTKE, M. 1982. Senckenberg-Grabungen in der Grube Messel bei Darmstadt – 3. Ergebnisse 1979–1981. *Courier Forschungsinstitut Senckenberg* **54**, 1–118.

FRANZEN, J. L. & HAUBOLD, H. 1986. The Middle Eocene of European mammalian stratigraphy. Definition of the Geiseltalian. *Modern Geology* **10**, 159–70.

GOTH, K., DE LEEUW, J. W., PÜTTMANN, W. & TEGELAAR, E. W. 1988. Origin of Messel oil shale kerogen. *Nature* **336**, 759–61.

GOTH, K. 1990. Der Messeler Ölschiefer – ein Algenlaminit. *Courier Forschungsinstitut Senckenberg* **131**, 1–143.

HANSGIRG, A. 1888. Prodromus der Algenflora von Böhmen. Erster Theil enthaltend die Rhodophyceen, Phaeophyceen und einen Theil der Chlorophyceen. *Archiv für die naturwissenschaftliche Landesdurchforschung von Böhmen* **6**(5), 109 + 97–288 [–290]. Prague.

HARMS, F.-J., ADERHOLD, G., HOFFMANN, I., NIX, T. & ROSENBERG, F. 1999. Erläuterungen zur Grube Messel bei Darmstadt (Südhessen). *Schriftenreihe der Deutschen Geologischen Gesellschaft* **8**, 181–222.

HEIL, R. 1964. Kieselschwamm-Nadeln im Ölschiefer der Grube Messel bei Darmstadt. *Notizblatt des Hessischen Landesamtes für Bodenforschung* **92**, 60–7.

HOLLOWAY, C. F. & COWAN, J. P. 1997. Development of a scanning confocal laser microscopic technique to examine the structure and composition of marine snow. *Limnology and Oceanography* **42**, 1340–52.

IRION, G. 1977. Der eozäne See von Messel. *Natur und Museum* **107**(7), 213–18.

JANKOWSKI, B. & LITTKE, R. 1986. Das organische Material der Ölschiefer von Messel. *Geowissenschaften in unserer Zeit* **4**(3), 73–80.

KEHREL, D. 1999. *Leica TCS confocal system user manual.* Leica Microsystems Heidelberg, Revision 9901, 149 pp.

KEMP, A. E. S., PEARCE, R. B., PIKE, J. & MARSHALL, J. E. A. 1998. Microfabric and microcompositional studies of Pliocene and Quaternary sapropels from the Eastern Mediterranean. *Proceedings of the Ocean Drilling Program, Scientific Results* **160**, 333–48.

MATTHESS, G. 1966. Zur Geologie des Ölschiefervorkommens von Messel bei Darmstadt. *Abhandlungen des Hessischen Landesamtes für Bodenforschung* **51**, 87 pp.

MACQUAKER, J. H. S. & GAWTHORPE, R. I. 1993. Mudstone lithofacies in the Kimmeridge Clay Formation, Wessex Basin, Southern England: implications for the original controls of the distribution of mudstones. *Journal of Sedimentary Petrology* **63**, 1129–43.

NIX, T. & FELDER, M. 2002. Weltnaturerbe Grube Messel. *Schriftenreihe der Deutschen Geologischen Gesellschaft* **18**, 45–57.

NORTON, T. A., THOMPSON, R. C., POPE, J., VELTKAMP, C. J., BANKS, B., HOWAR, C. V. & HAWKINS, S. J. 1998. Using confocal laser scanning microscopy, scanning electron microscopy and phase contrast light microscopy to examine marine biofilms. *Aquatic Microbial Ecology* **16**, 199–204.

PAWLEY, J. B. 1995. *Handbook of biological confocal microscopy.* 2nd ed. New York: Plenum Press.

REIMER, L. 1998. *Scanning Electron Microscopy – physics of image formation and microanalysis.* 2nd ed. Berlin, Heidelberg, New York: Springer, 527 pp.

RULLKÖTTER, J., LITTKE, R., HAGEDORN-GÖTZ, I. & JANKOWSKI, B. 1988. Vorläufige Ergebnisse der organisch-geochemischen und organisch-petrographischen Untersuchungen an Kernproben des Messeler Ölschiefers. *Courier Forschungsinstitut Senckenberg* **107**, 37–51.

SCHAAL, S. & ZIEGLER, W. 1992. *Messel – an insight into the life and history of the earth.* Oxford: Clarendon Press, 322 pp.

SHEPPARD, C. J. R. & SHOTTON, D. M. 1997. Confocal laser scanning microscopy. *Royal Microscopical Society Microscopy Handbooks* **38**, 106 pp.

STEVENS, J. K., MILLS, L. R. & TROGADIS, J. E. 1994. *Three-dimensional confocal microscopy. Volume investigation of biological systems.* London: Academic Press, 500 pp.

WEBER, J. & HOFMANN, U. 1982. Kernbohrungen in der eozänen Fossilienlagerstätte Grube Messel. *Geologische Abhandlungen Hessen* **83**, 58 pp.

WILDE, V. & SCHAARSCHMIDT, F. 1993. Neue Möglichkeiten zur Untersuchung von Pollen in situ an Pflanzenresten aus dem "Ölschiefer" von Messel. *Mitteilungen aus Wissenschaft und Technik* **10**(6), 209–14.

https://doi.org/10.1017/S0016756803008094 Published online by Cambridge University Press